Independent geometrical control of spin and charge resistances in curved spintronics

DOI:
10.1021/acs.nanolett.9b01994

Document Version
Accepted author manuscript

Independent geometrical control of spin and charge resistances in curved spintronics

Kumar Sourav Das,[1, a)] Denys Makarov,[2] Paola Gentile,[3] Mario Cuoco,[3] Bart J. van Wees,[1] Carmine Ortix,[4, 5, b)] and Ivan J. Vera-Marun[6, c)]

[1)] *Physics of Nanodevices, Zernike Institute for Advanced Materials, University of Groningen, 9747 AG Groningen, The Netherlands*

[2)] *Helmholtz-Zentrum Dresden-Rossendorf e.V., Institute of Ion Beam Physics and Materials Research, Bautzner Landstrasse 400, 01328 Dresden, Germany*

[3)] *CNR-SPIN and Dipartimento di Fisica "E. R. Caianiello", Università degli Studi di Salerno, I-84084 Fisciano, Italy*

[4)] *Institute for Theoretical Physics, Center for Extreme Matter and Emergent Phenomena, Utrecht University, Princetonplein 5, 3584 CC, Utrecht, The Netherlands*

[5)] *Institute for Theoretical Solid State Physics, IFW Dresden, 01171 Dresden, Germany*

[6)] *School of Physics and Astronomy, University of Manchester, Manchester M13 9PL, United Kingdom*

Spintronic devices operating with pure spin currents represent a new paradigm in nanoelectronics, with higher energy efficiency and lower dissipation as compared to charge currents. This technology, however, will be viable only if the amount of spin current diffusing in a nanochannel can be tuned on demand while guaranteeing electrical compatibility with other device elements, to which it should be integrated in high-density three-dimensional architectures. Here, we address these two crucial milestones and demonstrate that pure spin currents can effectively propagate in metallic nanochannels with a three-dimensional curved geometry. Remarkably, the geometric design of the nanochannels can be used to reach an independent tuning of spin transport and charge transport characteristics. These results put the foundation for the design of efficient pure spin current based electronics, which can be integrated in complex three-dimensional architectures.

Keywords: spintronics, non-local spin valves, curved nanoarchitectures, geometrical control, electrical and spin resistance

A number of next-generation electronic devices, including memory elements and transistor circuits, rely on spin currents. Pure spin currents[1–7] transfer only spin angular momentum and therefore have the additional advantage that the electronic devices can operate with low power dissipation. A pure spin current can be generated using the coupling between charge and spin transport across the interface of a ferromagnet with a contiguous paramagnetic nanochannel. The efficiency of the spin injection across this interface can be optimized by improving the interface quality and the device structure. The propagation of the pure spin current along the nanochannel is instead related to its spin relaxation length. In conventional metals and small-gap semiconductors, the dominant spin relaxation mechanism corresponds to the so-called Elliot-Yafet mechanism,[4,8,9] which dictates that the spin relaxation length is strictly locked to the resistivity of the metallic paramagnet. This, in turn, severely compromises the applicability of pure spin currents to technologically relevant modern electronics, which necessitates the individual matching of spin and charge resistances in order to achieve efficient coupling of spin and charge degrees of freedom.[8,10,11]

Here, by using a combination of experimental investigations and theoretical analysis, we show that spin and charge resistances can be independently tuned in metallic nanochannels. Importantly, this is realised even in the absence of any external electric or magnetic gating,[12,13] and it is totally different in nature to the spin-charge separation phenomenon in Tomonaga-Luttinger liquids.[14,15] Our strategy relies on the possibility to grow metallic nanochannels with a strongly inhomogeneous nanometer-scale thickness, t. The size-dependent resistivity, ρ, of the metallic channels[16] yields a different local behaviour for the sheet resistance ρ/t and the spin relaxation length $\lambda \propto 1/\rho$ [c.f. Fig. 1(a-c)]. As a result, an appropriate engineering of the nanochannel thickness allows to design nanochannels where one can achieve independent tuning of spin resistance without affecting the total charge resistance, and *vice versa*. This capability allows for the design of an element with simultaneous matching of spin resistance to a spin-based circuit, e.g. for efficient spin injection,[8,10,11] and matching of charge resistance to a charge-based circuit, e.g. for efficient power transfer. The control of spin and charge resistances is fundamental to spintronics, as it enables practical magnetoresistance in two terminal devices[17] and the concatenability and reduced feedback in spin logic architectures.[18,19]

[a)] e-mail: K.S.Das@rug.nl
[b)] e-mail: C.Ortix@uu.nl
[c)] e-mail: ivan.veramarun@manchester.ac.uk

As a proof of concept, we demonstrate modulation of spin currents and of charge currents in lateral non-local spin valves[1] with ultrathin metallic channels directly grown on curved templates [c.f. Fig. 1(d,e)], thereby allowing us to achieve efficient spin current propagation in three-dimensional nanoarchitectures. This is of immediate relevance when considering a practical implementation of spintronics. On the one hand, transport of pure spin currents in non-local spin valves is at the heart of multiple proposals of spin-based logic architectures,[18,19] and thus of potential technological impact. On the other hand, the use of curvature to independently control spin and charge impedances in multi-terminal devices adds a novel approach for their efficient integration with complementary metal oxide semiconductor (CMOS) transistors that optimizes device reliability and endurance.[20] Finally, as CMOS technology scales down to 10 nm features or less, there are increasing efforts in the development of three-dimensional CMOS microelectronics that can overcome the limitations of Moore's law. This is similar with regards to spintronics and its integration with CMOS. Such efforts have been led by the thinning and 3D stacking of several chips, initially integrating CMOS and spin-based memories[21] and later extended to heterogeneous chips.[22] A completely different approach is to change the architecture itself to be three-dimensional. Until now, the realisation of vertical flow of spin information via three-dimensional channels has been based solely on the movement of magnetic domain walls, by applying current[23] or magnetic field,[24] with a recent implementation based on depositing magnetic material on the sidewall of deep trenches.[25] Our work on curved nanoarchitectures for pure spin current devices delves into territory so far only explored for charge-based technologies. While being conceptually simple and potentially cheap, it offers the possibility of high density three-dimensional integration over that in conventional spin current devices.

Curved templates were created in the form of trenches in a silicon dioxide substrate. Increasing the height of the trenches A [c.f. Fig. 1(d,e)] led to channels with increasing curvature, allowing us to systematically explore the effect of channel geometry. To create the trenches we used focused ion beam (FIB) etching, where the geometry of the trenches was controlled by varying the FIB milling times. Each sample consists of two lateral spin valve devices: one device with the spin transport channel across the trench, resulting in a curved device, and another on the flat part of the substrate, serving as a reference device. The spin valve devices were prepared by multi-step e-beam lithography, e-beam evaporation of materials and resist lift-off techniques, as described in Ref. 26. Permalloy ($Ni_{80}Fe_{20}$, Py) nanowires, with a thickness of 20 nm, were used as the ferromagnetic electrodes. Injector and detector Py electrodes were designed with different widths (80 nm and 100 nm) to achieve different coercive fields. The injector-detector in-plane separation (L) was 500 nm for all the devices, except for the one with the largest trench height ($A = 270$ nm) which had a separation of 700 nm. For the spin transport channel we used an aluminium (Al) nanowire, with a width of 100 nm and a nominal thickness of 50 nm. The Al channel was evaporated following a short in-situ ion milling step to remove surface oxide and resist contamination from the Py electrodes, resulting in Al/Py ohmic contacts with a resistance-area product lower than 10^{-15} $\Omega.m^2$. Fig. 1(f) shows a scanning electron microscope image of one of the fabricated curved spin valve devices.

All electrical measurements were performed with the sample in a high vacuum environment, within a liquid helium cryostat. The electrical resistance of the Al channel was measured by the four-probe method, with the current applied between the two ends of the Al channel and the voltage drop measured between the injector and the detector electrodes. For the non-local spin valve measurements, the electrical connections are schematically shown in Fig. 1(f). Here, an alternating current (I) source, with a magnitude of 400 μA and frequency of 13 Hz, was connected between the injector electrode and the left end of the Al channel. The non-local voltage (V) at the detector electrode, with reference to the right end of the Al channel, was measured by a phase sensitive lock-in technique. A magnetic field was applied along the length of the Py wires during these measurements to configure the injector and detector electrodes in a parallel (P) or an anti-parallel (AP) state, corresponding to two distinct levels of the non-local resistance ($R_{NL} = V/I$). The spin valve signal (ΔR_{NL}) is then given by the difference of the non-local resistance between parallel and anti-parallel configurations, $\Delta R_{NL} = R_{NL}^{P} - R_{NL}^{AP}$. The measurements were carried out at room temperature and at 4.2 K to study spin transport in channels with increasing curvature. The extraction of ΔR_{NL} via this standard low-frequency first-harmonic lock-in technique serves to accurately extract the pure spin current signal and exclude any role of induction or thermoelectric effects.[1,26]

The non-local spin valve measurements are shown in Fig. 2(a). The resulting modulation of ΔR_{NL} with A is plotted in Fig. 2(b). ΔR_{NL} is maximum for the reference spin valves with $A = 0$ and shows little change for trenches with $A < 50$ nm, limited by device to device variation. However, for increasing trench heights above ≈ 100 nm we observe a strong decrease in ΔR_{NL}, until it is fully suppressed for the trench with $A = 270$ nm. On the other hand, the measured four-probe charge resistance of the curved channel between the injector and detector electrodes exhibited an opposite trend, as observed in Fig. 2(c). Here, a steep increase in resistance (R) is seen for trenches with height greater than ≈ 100 nm. A similar behaviour was observed at room temperature [see Supporting Information Section 1].

The contrasting behaviours of both the spin valve signal and charge resistance offer direct evidence of the effect of the curved geometry introduced by the trench. We have first checked that both the strong suppression of ΔR_{NL} and the steep increase of R with increasing A cannot be explained just by considering the increase in

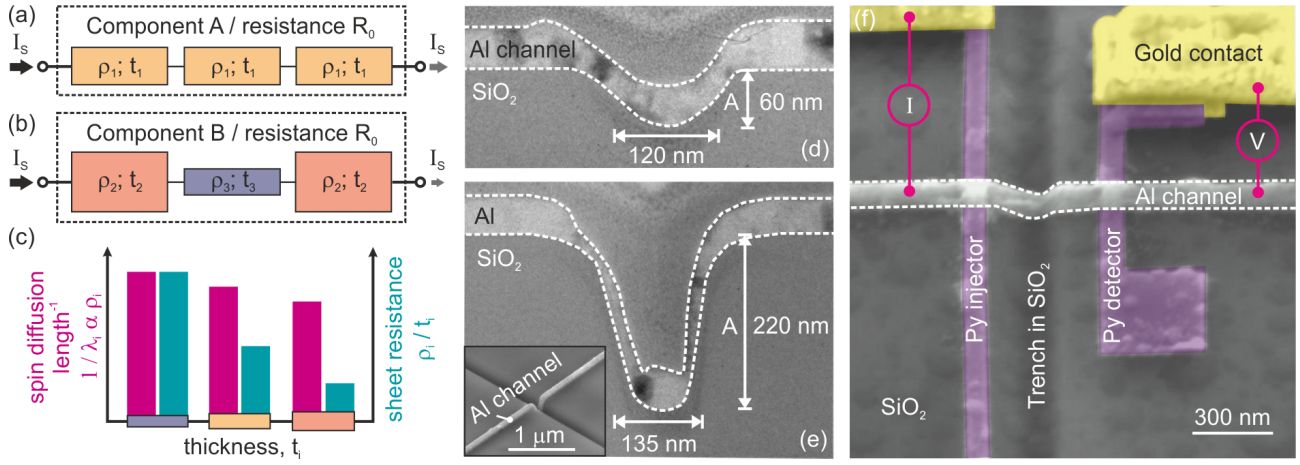

FIG. 1. **Concept of geometrical control of spin current and curved device architecture. (a-b)** Schematics of two different spin transport channels, each composed of three elements in series. The elements of the channel in (a) are identical, representing a homogeneous channel, resulting in a total charge resistance R_0 and a spin current I_s. The channel in (b) is inhomogeneous, with components having different thicknesses and resistivities (ρ), and still with a total charge resistance R_0. However, its spin resistance is differently modulated with the thickness, resulting in a different spin current as compared to the homogeneous channel in (a). **(c)** Distinct role of channel thickness (t) on the modulation of sheet resistance ρ/t and of the spin relaxation length (λ), leading to distinct scaling of charge and spin resistances. **(d-e)** Transmission electron microscope (TEM) cross-sections of Al channels grown on trenches of different geometries, characterized by the trench height A and the full width at half maximum. Top-view of an Al channel grown across a trench is shown in the scanning electron microscope (SEM) image in the inset of panel (e). **(f)** SEM image of a spin valve device with a curved Al channel across a trench. The electrical connections for non-local spin valve measurements are also depicted.

the channel length due to the curved geometry. To properly describe both of these behaviours we have therefore developed a theoretical model which is applicable to devices, where the local channel geometry explicitly impacts on both charge and spin transport properties. Here the key ingredient is the consideration of the dominant Elliot-Yafet spin relaxation mechanism. The main outcome of this approach is depicted by the dotted lines in Fig. 2(b-c), where *quantitative* agreement with the experimental results is achieved. In the following discussion we introduce this theoretical model.

To develop an accurate description of the channel we rely on the knowledge of its geometry from TEM imaging (Fig. 1). We observe how at the steep walls of the trench the film thickness was reduced, relative to its nominal thickness. This variation in thickness is determined by the e-beam evaporation technique used to grow the film, where nominal thickness is only achieved when the Al beam impinges on the substrate at normal incidence. With this direct evidence of thickness inhomogeneity, we have incorporated it in our description of the curved channel by modelling the trench profile as a Gaussian bump with FWHM of ≈ 100 nm, as shown in Fig. 3(a). The resulting thickness of the Al channel in the local surface normal direction $\hat{n}$ then becomes intrinsically inhomogeneous. We describe the Gaussian bump as $h(x) = Ae^{-x^2/(2\sigma^2)}$, where the x coordinate is measured with respect to the maximum trench height position. We next consider that the top surface of the evaporated Al film assumes the same profile with $h_T(x) = t_0 + h(x)$, and

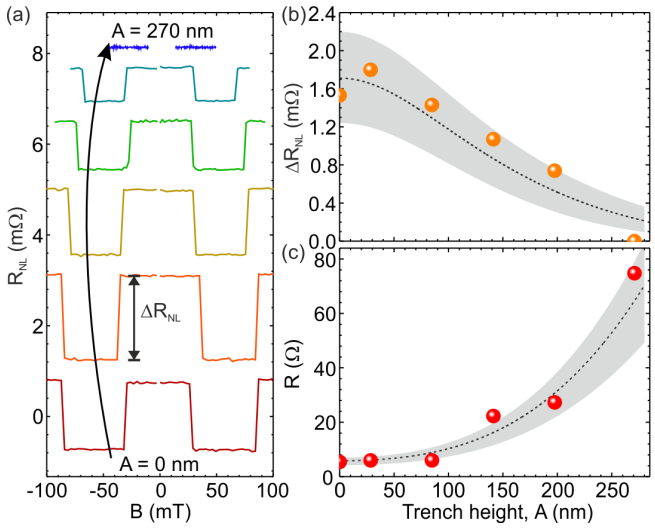

FIG. 2. **Non-local spin valve signal and channel resistance measurements and modelling. (a)** Spin valve measurements at $T = 4.2$ K for devices with different channel geometries. The black arrow indicates the direction of increasing trench height, A. The spin signal $\Delta R_{\rm NL}$ decreases with increasing A. **(b)** $\Delta R_{\rm NL}$ as a function of A. The experimental data and the modelling result are shown as solid spheres and dotted line, respectively. The shaded region in grey represents the uncertainty due to device to device variation. **(c)** Experimental data and modelling results for the charge resistance (R) of the channel, for different A.

t_0 the nominal thickness. With this, the total volume of the evaporated Al channel does not depend on the geometry of the trench, and it is given by $t_0 L w$ where w is the channel width, and L the distance in the $\hat{x}$ coordinate between injector and detector. In order to subsequently derive the local thickness profile, we write the line element

$$ds^2 = \left[1 + \left(\frac{dh(x)}{dx}\right)^2\right] dx^2,$$

which allows to express the arclength measured from the injector electrode as

$$s(x) = \int_{-L/2}^{x} \sqrt{1 + \left(\frac{dh(x')}{dx'}\right)^2}. \tag{1}$$

The channel length between injector and detector is given by $L' \equiv s(L/2)$. Furthermore, the local thickness profile can be obtained by requiring $\int_0^{L'} t(s)ds \equiv t_0 L$. This relation is satisfied for a local thickness profile, which, in terms of the x coordinate can be expressed as

$$t(x) = \frac{t_0}{\sqrt{1 + \left(\frac{\partial h(x)}{\partial x}\right)^2}}.$$

The equation above in combination with Eq. 1 correspond to the parametric equations for the local thickness $t(s)$. This, in turn, allows to find the local behaviour of the resistivity $\rho(t)$. The total charge resistance of the Al channel can be then calculated by using $R = \int_0^{L'} \rho(s)/[t(s)w]ds$.

A proper modelling of the charge and spin transport properties therefore requires to explicitly consider the thickness dependence of the resistivity.[16] We do so by employing the Mayadas-Shatzkes (MS) model,[27] which accounts for the increase of electrical resistivity of the thin channel due to electron scattering at grain boundaries. Assuming that the thickness in the local surface normal of the Al channel corresponds to the smallest dimension between grain boundaries, the MS model provides us with a functional form of the resistivity as a function of the thickness, reading:

$$\frac{\rho_0}{\rho(t)} = 3\left[\frac{1}{3} - \frac{\alpha}{2} + \alpha^2 - \alpha^3 \log\left(1 + \frac{1}{\alpha}\right)\right], \tag{2}$$

where ρ_0 is the resistivity of bulk Al, and $\alpha = \lambda_{\mathbf{e}} C/[t(1-C)]$ can be determined from the knowledge of the electronic mean free path, $\lambda_{\mathbf{e}}$, and the empirical reflectivity coefficient, C. We estimate the latter by using the value of the room-temperature mean free path $\lambda_{\mathbf{e}} = 18.9$ nm and bulk Al resistivity $\rho_0 = 2.65 \times 10^{-8}\,\Omega\,\mathrm{m}$,[28] and our experimental average resistivity at room temperature for reference Al channels of nominal thickness, $\rho(t_0) = 8.9 \times 10^{-8}\,\Omega\,\mathrm{m}$. We thereby obtain a reflectivity coefficient $C \simeq 0.82$. For the reference devices, we got a device to device statistical variance of $\approx 2\,\Omega$, of the same size as the symbol for $A = 0$ in Fig. 2(c). A statistical variance in the reflectivity coefficient of ± 0.04 allows us to account for this device to device variation. Considering the scattering related to grain boundaries to be temperature independent, the obtained reflectivity coefficient can be further used to model the thickness dependent resistivity at low temperature, which we calibrate using our experimental average resistivity for reference channels at 4.2 K, $\rho(t_0) = 5.6 \times 10^{-8}\,\Omega\,\mathrm{m}$. The values of resistivities considered above are consistent with the range of values observed for thin Al films in previous studies.[26] The ensuing behaviour of the charge resistance as a function of the trench height fits nicely with our experimental results [c.f. Fig. 2(c)].

To obtain the inhomogeneous profile of the spin relaxation length, we use the fact that the latter can be expressed as $\lambda = \sqrt{\tau_s D}$, where D is the diffusion coefficient and τ_s is the spin relaxation time. Using the Einstein relation, $D = 1/(\rho\, e^2\, N_{\mathrm{Al}})$, with N_{Al} the density of states in the channel at the Fermi level, we can therefore predict the thickness dependence of the diffusion constant. Moreover, the Elliot-Yafet mechanism predicts a scaling of the spin relaxation time, $\tau_s \propto \tau_p \propto 1/\rho$, where τ_p is the momentum relaxation time. These considerations yield $\lambda \propto \rho^{-1}$, and allow to consider the ansatz for the thickness dependence of the spin relaxation length $\lambda(t) = \lambda_0 \rho_0/\rho(t)$, whose functional form is uniquely determined by Eq. 2, while the unknown λ_0 is fixed by requiring the spin relaxation length at the nominal thickness to be equal to that measured in reference devices, $\lambda_0 = 660$ nm at 4.2 K.[26] The ensuing spin relaxation length along the curved Al channel is shown in Fig. 3(b), with a behaviour that is clearly inverse to that of the resistivity.

The spin valve signal is determined by the spin relaxation length and resistivity of the channel, which are both intrinsically inhomogeneous. This intrinsic inhomogeneity impedes the calculation of the spin signal using the simple analytical framework originally introduced by Takahashi and Maekawa for homogeneous channels.[29] For this reason, we have thereby extended the model by fully taking into account the inhomogeneity of the spin relaxation length along the channel [see Supporting Information Sections 2 and 3]. With this approach, we find a closed expression for the spin accumulation signal in the ohmic contact regime, which reads:

$$\Delta R_{\mathrm{NL}} = \frac{4p_{\mathrm{F}}^2}{(1-p_{\mathrm{F}}^2)^2} \frac{\mathcal{R}_{\mathrm{F}}^2}{\mathcal{R}_{\mathrm{N}}} \frac{e^{-\int_0^{L'} \frac{1}{\lambda_{\mathrm{N}}(s')} ds'}}{1 - e^{-2\int_0^{L'} \frac{1}{\lambda_{\mathrm{N}}(s')} ds'}}, \tag{3}$$

where w is the channel width, L' is the distance between injector and detector along the arclength $\hat{s}$, λ_{N} is the equal spin relaxation length at the injector and detector, $\mathcal{R}_{\mathrm{N}} = \rho_{\mathrm{N}}\lambda_{\mathrm{N}}/wt$, $\mathcal{R}_{\mathrm{F}}$ is the resistance of the ferromagnetic electrode with length λ_{F} (λ_{F} being the corresponding spin relaxation length), and p_{F} is the current

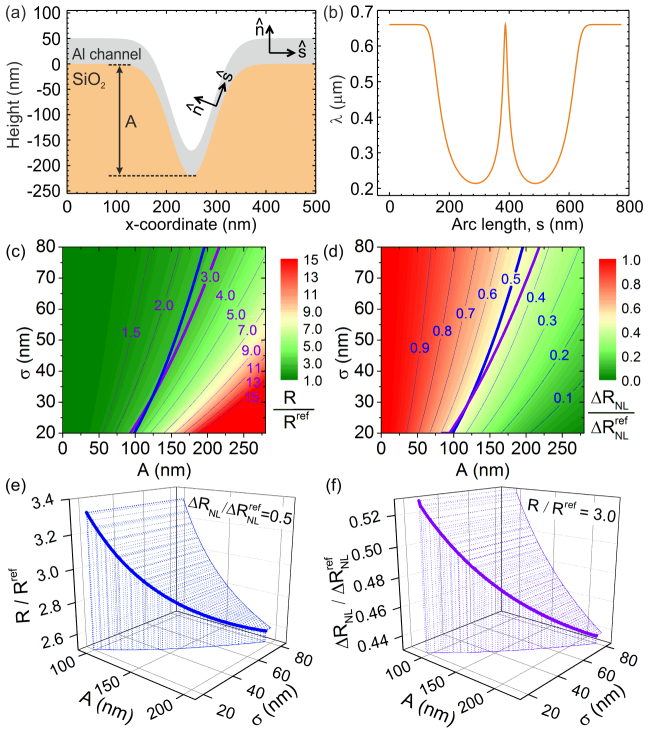

FIG. 3. **Geometry-induced tuning of charge resistance and spin resistance.** **(a)** The trench geometry is modelled as a Gaussian bump and the profile of the Al channel across the trench is mapped out. The trench height (A) and the unit vector $\hat{s}$ along the arclength of the Al film, perpendicular to the local surface normal $\hat{n}$, have been illustrated. **(b)** Calculated variation of the spin relaxation length in Al along s at 4.2 K. **(c-d)** 2D colour maps illustrating the modulation of charge resistance (c) and spin resistance (d) with the channel geometry, considering a template in the form of a Gaussian bump with height A and full width at half maximum $2\sqrt{2\log 2}\sigma$ as that in (a). Both the charge (R) and the spin ($\Delta R_{\rm NL}$) resistances have been normalized by the respective values for a reference flat channel. A contour line representing $R/R^{\rm ref} = 3.0$ (thick black) in panel (c) has been projected onto panel (d), and a contour line representing $\Delta R_{\rm NL}/\Delta R_{\rm NL}^{\rm ref} = 0.5$ (thick blue) in panel (d) has been projected onto panel (c). **(e)** 3D plot of the contour line for $\Delta R_{\rm NL}/\Delta R_{\rm NL}^{\rm ref} = 0.5$ mapped onto the values of $R/R^{\rm ref}$ from panel (c). **(f)** A similar 3D plot of the contour line representing $R/R^{\rm ref} = 3.0$ mapped onto the values of $\Delta R_{\rm NL}/\Delta R_{\rm NL}^{\rm ref}$ from panel (d). These results highlight the independent tuning of spin resistance for a constant charge resistance, and *vice versa*, via nanoscale design of the template geometry.

polarization of the ferromagnetic electrodes. The latter two quantities can be obtained from the spin signal in reference flat devices. Therefore, the knowledge of the local behaviour of the spin relaxation length allows us to obtain $\Delta R_{\rm NL}$ as a function of the trench height. For the case of a homogeneous channel the integral in the exponents simplify to $L/\lambda_{\rm N}$ and Eq. 3 reproduces the usual theory.[29] By considering the same statistical variance in the reflectivity coefficient, C, derived from the charge transport above, we find a striking agreement between the theoretical results and the experimental spin valve data, as shown in Fig. 2(b). The latter serves as experimental validation of our generalized diffusive spin transport model for inhomogeneous channels here presented. This in turn allows us to identify the dominant physical properties controlling spin transport in three-dimensional architectures, where inhomogeneity is directly controlled by the local geometry.

The analytical expression obtained in Eq. 3 allows us to interrogate in an efficient manner a broader phase space of geometrical variations of curved templates, e.g. as the Gaussian bumps described in Fig. 3(a-b). The resulting 2D maps for charge resistance and spin resistance, due to the exploration of the phase space of Gaussian bump height A and full width at half maximum $2\sqrt{2\log 2}\sigma$, are shown in Fig. 3(c-d). A key observation is the distinct scaling of the charge resistance and the spin resistance due to geometric control, evidenced by the different contour lines in both 2D maps. We highlight this difference by mapping a contour line from each 2D map into the other, resulting in 3D plots shown in Fig. 3(e-f). Here, we observe the direct tuning of spin resistance independent of the charge resistance, and *vice versa*, via the nanoscale design of the template geometry. This hitherto unexplored approach to control the ratio of spin resistance to charge resistance, even within a single material system, has the potential to aid in the design of future circuits based on pure spin currents.[8]

Our curved-template approach enables control of the ratio of spin resistance to charge resistance in individual nanochannels, while allowing the fabrication of a spintronic architecture via a single deposition of the channel material. For flat homogeneous nanochannels the need of multiple deposition steps for each desired thickness would rapidly lead to an impractical fabrication process. Therefore, it is relevant to consider how simply tuning the length in flat homogeneous nanochannels, which is practical via lithography, compares with curved inhomogeneous nanochannels at the same nominal thickness. For a flat nanochannel to achieve a charge resistance $R/R^{\rm ref} = 3.0$, its length must be increased to 3 times that of a reference channel, which leads to a spin resistance[29] of only $\Delta R_{\rm NL}/\Delta R_{\rm NL}^{\rm ref} = 0.17$. This is significantly lower than the value of up to 0.52 obtained in Fig. 3(f), and is one example of the general advantage offered by curved inhomogeneous channels for efficient individual control of spin and charge resistances [see Supporting Information Sections 4 and 5]. Spatial inhomogeneity below the characteristic length scale for spin transport, FWHM $\lesssim \lambda$, combined with control of thickness down to the characteristic length scale for charge transport, $t \lesssim \lambda_e$, has been a hitherto unrecognised physical approach to enable such an efficient control within the context of Elliot-Yafet spin relaxation.[4,8,9]

Using lateral non-local spin valves, we have demonstrated that an appropriate geometric design of metallic nanochannels yields spin resistance changes at constant electrical resistance and *vice versa*. Although spa-

tially inhomogeneous nanochannels can be created in planar structures,[30] our approach, using three-dimensional nanoarchitectures with a designed curved profile, intrinsically provides the necessary control to achieve the independent tuning of spin and charge resistances. Note that for planar structures there are other methods for controlling spin and charge currents. These rely on novel nanoscale materials, or heterostructures thereof, to gain functionality by active use of electric field,[31–34] drift current[35,36] or proximity-induced spin relaxation.[37,38] Such methods are highly relevant for current research, though their integration with current technologies is limited by their requirement of novel materials or low temperatures. In contrast, we expect our geometrical approach to be completely generic and thus applicable to other non-magnetic materials exhibiting a dominant Elliot-Yafet spin relaxation mechanism, e.g. Cu, or heterostructures thereof.[4,9,30] The combination of geometrical control and novel nanoscale materials is an interesting avenue for future spintronic technologies.

Recent works have explored technologically relevant curvilinear nanoarchitectures that transport vertically domain walls for magnetologic applications.[23,25] Others have used curved templates pre-structured via self-assembly of nanostructures, which allows the nanoscale tuning of microstructure, thickness, and magnetic anisotropy of the deposited magnetic curved films.[39] Geometrical effects can trigger new functionalities both in semiconducting[40–44] and superconducting[45] low-dimensional systems. The geometrical control of pure spin currents demonstrated in this work can thus inaugurate the search for novel effects in spintronic devices using other ultrathin curved materials like semiconductors and superconductors.

ASSOCIATED CONTENT

Supporting Information

The Supporting Information is available free of charge on the ACS Publications website at http://pubs.acs.org.

AUTHOR INFORMATION

Corresponding Authors

Correspondence and requests for materials should be addressed to K.S.D., C.O. and I.J.V.M.

Author Contributions

C.O., P.G., D.M., I.J.V.M. conceived and supervised the project. I.J.V.M. and K.S.D. conceived and designed the experiments. K.S.D. carried out the experiments and the initial data analysis. D.M. supplied the curved templates and the corresponding electron microscopy imaging. C.O. developed and performed the theoretical analysis with the help of P.G. and M.C.. K.S.D., C.O. and I.J.V.M. performed the final data analysis and wrote the manuscript with the help of B.J.v.W., M.C., P.G., and D.M. All authors discussed the results and the manuscript.

Notes

The authors declare no competing financial interest.

ACKNOWLEDGMENTS

We thank Dr. S. Baunack (IFW Dresden) for his contribution at the initial stage of this work and J. G. Holstein, H. M. de Roosz, H. Adema and T. Schouten for their technical assistance. Support by the Structural Characterization Facilities at IBC of the HZDR is gratefully acknowledged. We acknowledge the financial support of the Zernike Institute for Advanced Materials and the Future and Emerging Technologies (FET) programme within the Seventh Framework Programme for Research of the European Commission, under FET-Open Grant No. 618083 (CNTQC). C.O. acknowledges support from the Deutsche Forschungsgemeinschaft (Grant No. OR 404/1-1), and from a VIDI grant (Project 680-47-543) financed by the Netherlands Organization for Scientific Research (NWO). D.M. acknowledges support from the ERC within the EU 7th Framework Programme (ERC Grant No. 306277).

REFERENCES

[1] Jedema, F. J.; Filip, A. T.; van Wees, B. J. *Nature* **2001**, *410*, 345–348.
[2] Valenzuela, S. O.; Tinkham, M. *Appl. Phys. Lett.* **2004**, *85*, 5914–5916.
[3] Kimura, T.; Otani, Y. *Phys. Rev. Lett.* **2007**, *99*, 196604.
[4] Kimura, T.; Sato, T.; Otani, Y. *Phys. Rev. Lett.* **2008**, *100*, 066602.
[5] Lou, X.; Adelmann, C.; Crooker, S. A.; Garlid, E. S.; Zhang, J.; Reddy, K. S. M.; Flexner, S. D.; Palmstrøm, C. J.; Crowell, P. A. *Nature Phys.* **2007**, *3*, 197–202.
[6] van 't Erve, O. M. J.; Hanbicki, A. T.; Holub, M.; Li, C. H.; Awo-Affouda, C.; Thompson, P. E.; Jonker, B. T. *Appl. Phys. Lett.* **2007**, *91*, 212109.
[7] Tombros, N.; Jozsa, C.; Popinciuc, M.; Jonkman, H. T.; van Wees, B. J. *Nature* **2007**, *448*, 571–574.
[8] Žutić, I.; Fabian, J.; Das Sarma, S. *Rev. Mod. Phys.* **2004**, *76*, 323–410.
[9] Jedema, F. J.; Nijboer, M. S.; Filip, A. T.; van Wees, B. J. *Phys. Rev. B* **2003**, *67*, 085319.
[10] Schmidt, G.; Ferrand, D.; Molenkamp, L. W.; Filip, A. T.; van Wees, B. J. *Phys. Rev. B* **2000**, *62*, R4790–R4793.
[11] Rashba, E. I. *Phys. Rev. B* **2000**, *62*, R16267.
[12] Villamor, E.; Isasa, M.; Vélez, S.; Bedoya-Pinto, A.; Vavassori, P.; Hueso, L. E.; Bergeret, F. S.; Casanova, F. *Phys. Rev. B* **2015**, *91*, 020403.
[13] Dejene, F. K.; Vlietstra, N.; Luc, D.; Waintal, X.; Ben Youssef, J.; van Wees, B. J. *Phys. Rev. B* **2015**, *91*, 100404.
[14] Giamarchi, T. *Quantum Physics in One Dimension*; International Series of Monographs on Physics; Oxford University Press: Oxford, New York, 2003.
[15] Tsvelik, A. M.; Yevtushenko, O. M. *Phys. Rev. Lett.* **2015**, *115*, 216402.
[16] Steinhögl, W.; Schindler, G.; Steinlesberger, G.; Engelhardt, M. *Phys. Rev. B* **2002**, *66*, 075414.

[17] Fert, A.; Jaffrès, H. *Phys. Rev. B* **2001**, *64*, 184420.
[18] Dery, H.; Dalal, P.; Cywiński, Ł.; Sham, L. J. *Nature* **2007**, *447*, 573–576.
[19] Behin-Aein, B.; Datta, D.; Salahuddin, S.; Datta, S. *Nat Nano* **2010**, *5*, 266–270.
[20] Makarov, A.; Windbacher, T.; Sverdlov, V.; Selberherr, S. *Semicond. Sci. Technol.* **2016**, *31*, 113006.
[21] M. Sekikawa,; K. Kiyoyama,; H. Hasegawa,; K. Miura,; T. Fukushima,; S. Ikeda,; T. Tanaka,; H. Ohno,; M. Koyanagi, *2008 IEEE International Electron Devices Meeting* **2008**, 1–3.
[22] M. Koyanagi, *2013 IEEE International Electron Devices Meeting* **2013**, 1.2.1–1.2.8.
[23] Parkin, S. S. P.; Hayashi, M.; Thomas, L. *Science* **2008**, *320*, 190–194.
[24] Lavrijsen, R.; Lee, J.-H.; Fernández-Pacheco, A.; Petit, D. C. M. C.; Mansell, R.; Cowburn, R. P. *Nature* **2013**, *493*, 647–650.
[25] Parkin, S. S. P.; Yang, S. H. *Nature Nano.* **2015**, *10*, 195–198.
[26] Das, K. S.; Dejene, F. K.; van Wees, B. J.; Vera-Marun, I. J. *Phys. Rev. B* **2016**, *94*, 180403.
[27] Mayadas, A. F.; Shatzkes, M. *Phys. Rev. B* **1970**, *1*, 1382–1389.
[28] Gall, D. *Journal of Applied Physics* **2016**, *119*, 085101.
[29] Takahashi, S.; Maekawa, S. *Phys. Rev. B* **2003**, *67*, 052409.
[30] Masourakis, E.; Arzubiaga, L.; Mihajlović, G.; Villamor, E.; Llopis, R.; Fèlix C.,; Hueso, L. E. *Nanotechnology* **2016**, *27*, 095201.
[31] Guimarães, M. H. D.; Zomer, P. J.; Ingla-Aynés, J.; Brant, J. C.; Tombros, N.; van Wees, B. J. *Phys. Rev. Lett.* **2014**, *113*, 086602.
[32] Avsar, A.; Vera-Marun, I. J.; Tan, J. Y.; Koon, G. K. W.; Watanabe, K.; Taniguchi, T.; Adam, S.; Özyilmaz, B. *NPG Asia Mater* **2016**, *8*, e274.
[33] Avsar, A.; Özyilmaz, B.; Fabian, J.; Tan, J. Y.; Watanabe, K.; Kurpas, M.; Gmitra, M.; Taniguchi, T. *Nature Physics* **2017**, *13*, 888.
[34] Lin, X.; Su, L.; Si, Z.; Zhang, Y.; Bournel, A.; Zhang, Y.; Klein, J.-O.; Fert, A.; Zhao, W. *Phys. Rev. Applied* **2017**, *8*, 034006.
[35] Ingla-Aynés, J.; Meijerink, R. J.; Wees, B. J. v. *Nano Lett.* **2016**, *16*, 4825–4830.
[36] Vera-Marun, I. J.; Ranjan, V.; van Wees, B. J. *Phys. Rev. B* **2011**, *84*, 241408(R).
[37] Yan, W.; Txoperena, O.; Llopis, R.; Dery, H.; Hueso, L. E.; Casanova, F. *Nat. Commun.* **2016**, *7*, 13372.
[38] Benítez, L. A.; Sierra, J. F.; Torres, W. S.; Arrighi, A.; Bonell, F.; Costache, M. V.; Valenzuela, S. O. *Nature Physics* **2018**, *14*, 303.
[39] Streubel, R.; Fischer, P.; Kronast, F.; Kravchuk, V. P.; Sheka, D. D.; Gaididei, Y.; Schmidt, O. G.; Makarov, D. *J. Phys. D: Appl. Phys.* **2016**, *49*, 363001.
[40] Gentile, P.; Cuoco, M.; Ortix, C. *Phys. Rev. Lett.* **2015**, *115*, 256801.
[41] Nagasawa, F.; Frustaglia, D.; Saarikoski, H.; Richter, K.; Nitta, J. *Nat. Commun.* **2013**, *4*.
[42] Ying, Z. J.; Gentile, P.; Ortix, C.; Cuoco, M. *Phys. Rev. B* **2016**, *94*, 081406.
[43] Gazibegovic, S.; Car, D.; Zhang, H.; Balk, S. C.; Logan, J. A.; de Moor, M. W. A.; Cassidy, M. C.; Schmits, R.; Xu, D.; Wang, G. et al. *Nature* **2017**, *548*, 434–438.
[44] Chang, C. H.; Ortix, C. *Nano Lett.* **2017**, *17*, 3076–3080.
[45] Turner, A. M.; Vitelli, V.; Nelson, D. R. *Rev. Mod. Phys.* **2010**, *82*, 1301–1348.